Using the s ensemble to probe glasses formed by cooling and aging

Aaron S. Keys, David Chandler, and Juan P. Garrahan

Phys. Rev. E **92**, 022304 — Published 12 August 2015

DOI: 10.1103/PhysRevE.92.022304

Using the s Ensemble to Probe Glasses Formed by Cooling and Aging

Aaron S. Keys[1,2], David Chandler[1] and Juan P. Garrahan[3*]
[1] *Department of Chemistry, University of California, Berkeley CA, 94720*
[2] *Lawrence Berkeley National Laboratory, Berkeley CA, 94720 and*
[3] *School of Physics and Astronomy, University of Nottingham, Nottingham, NG7 2RD, United Kingdom*

From length scale distributions characterizing frozen amorphous domains, we relate the s ensemble method with standard cooling and aging protocols for forming glass. We show that in a class of models where space-time scaling is in harmony with that of experiment, the spatial distributions of excitations obtained with the s ensemble are identical to those obtained through cooling or aging, but the computational effort for applying the s ensemble is generally many orders of magnitude smaller than that of straightforward numerical simulation of cooling or aging. We find that in contrast to the equilibrium ergodic state, a non-equilibrium lengthscale characterises the anti-correlation between excitations and encodes the preparation history of glass states.

I. INTRODUCTION

Through biasing statistics of trajectory space—the so-called "s ensemble" method—non-equilibrium phase transitions emerge between ergodic liquid-like states and dynamically inactive glass-like states. This class of transitions are found in idealized lattice models [1, 2] and in simulations of atomistic models [3–5]. In the latter case, it affords a systematic computational means of preparing exceptionally stable glass states [6]. This paper draws the conclusion that the s ensemble transition coincides with the physical glass transition [7], and the ensemble of its inactive states are those of natural structural glass. Specifically, we derive correspondence between spatial correlations in the s ensemble glass with those in the glass produced with finite-rate cooling or aging. The correspondence provides a basis for an extraordinarily efficient route for preparing structural glass with molecular simulations.

The equivalence that we put forward here between glasses prepared computationally via the s ensemble and those prepared through standard means such as cooling and aging is based on the detailed study of an idealised glass model, the East model [8, 9]. The East model is a spin facilitated model on the lattice with hierarchical dynamics leading to a super-Arrhenius relaxation law of the "parabolic" kind [9] (i.e., the exponential of a quadratic function of the inverse temperature). The East model captures many of the observed features of real glass formers [7] and its main physical ingredients of localised excitations and hierarchical dynamics can be seen to be present in more realistic liquid models [10]. The simplicity of the East model allows for detailed studies of its dynamics, which here we use to make predictions about the glass state more generally.

The paper is organised as follows. In Sec. II we consider the fluctuation properties of dynamical trajectories of atomistic liquid models in the supercooled regime accessible to simulations. Here we discuss the concept of excitations (or soft-spots) [10] that allows to establish the connection between atomistic systems and East-like models, together with the associated scaling laws obeyed by space-time fluctuations. This section contains one of our two central result: we demonstrates that rare space-time domains of low activity exhibit pronounced anti-correlation between excitations; this is a signature at the mesoscopic level of the anti-correlation between excitations that we argue later is typical of the glass.

In Sec. III we describe in general the three routes to prepare glasses, that is, materials which fall out of equilibrium due to their relaxation times exceeding the available observation time. Two of these routes are the standard ones of cooling and of aging after a quench. The third one is that of biasing the ensemble of trajectories by removing dynamical activity, i.e., that of the s ensemble method. Furthermore, we argue on general grounds, using the scaling ideas of Sec. II, that the glasses obtained through the standard procedures and the s ensemble should be equivalent. This is our second central result, and the validity of this prediction is tested explicitly in Sec. IV for the case of the East model. Section V provides our conclusions.

II. SPACE-TIME STRUCTURE OF GLASS-FORMING LIQUIDS

To begin, it is helpful to consider Figs. 1a and 1b, which render trajectories of a two-dimensional 5×10^4-particle system in a fashion that extends the approach of Ref. [10]. The system is a liquid mixture at a temperature that is 80% below that of the onset temperature, $T_{\rm o}$ [10–14], and the trajectory runs for an observation time $t_{\rm obs} \approx 10\,\tau$. Here, τ stands for the equilibrium structural relaxation time. It is about 10^5 integration steps at this particular temperature, and $t_{\rm obs}$, being 10 times longer, provides ample opportunity to observe the nature of dynamic heterogeneity in the system. The simulations illustrate correlated dynamics of a glass-forming material, which is distinct from dynamics of crystal coarsening (see Appendix A).

Most motions in glass-forming liquids are irrelevant vi-

* Corresponding author, Juan.Garrahan@nottingham.ac.uk

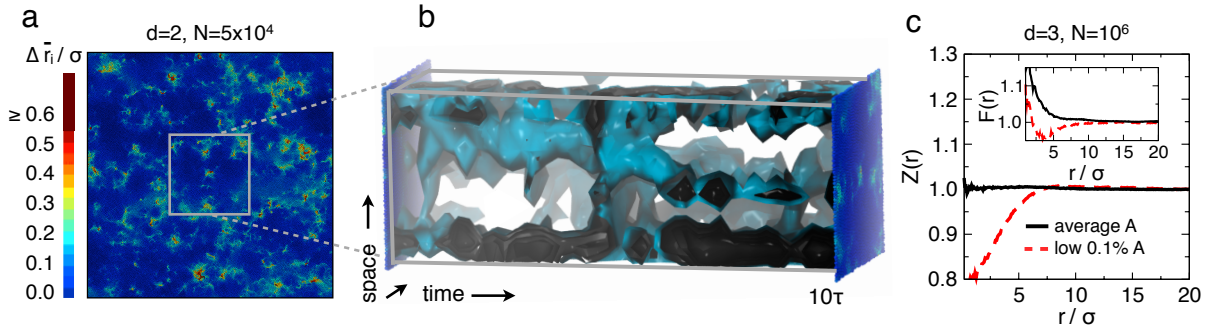

FIG. 1. (Color online) Soft spots and space-time bubbles. (a) Burnished excitations for the $d = 2$ supercooled WCA liquid mixture [10], with $\Delta\bar{r}_i = [|\bar{\mathbf{r}}_i(\Delta t) - \bar{\mathbf{r}}_i(0)|]_{\rm iso}$. (b) Excitation lines for a subsection of the system shown in (a). (c) The functions $Z(r)$ and $F(r)$ demonstrating correlation holes for inactive subsystems of a supercooled $d = 3$ WCA liquid mixture [23].

brations, and the amplitudes of most of those vibrations are similar in size to typical enduring displacements [10]. Irrelevant vibrations can be filtered out by focusing on inherent structures [15]. The set of particle positions at time t, $\{\mathbf{r}_i(t)\}$, evolves by molecular dynamics; the inherent structure, $\{\bar{\mathbf{r}}_i(t)\}$, is the position of the potential-energy minimum closest to $\{\mathbf{r}_i(t)\}$. The renderings in Fig. 1 refer to $[a(\mathbf{r}, t)]_{\rm iso}$, where

$$a(\mathbf{r}, t) = \sum_{i=1}^{N} |\bar{\mathbf{r}}_i(t + \Delta t) - \bar{\mathbf{r}}_i(t)|\, \delta(\mathbf{r} - \bar{\mathbf{r}}_i(t))\,. \qquad (1)$$

Here, we take Δt to be 10^3 integration steps, which is roughly the average time to complete an enduring displacement of one atomic diameter [10], and $[\cdots]_{\rm iso}$ indicates iso-configurational averaging, which averages many trajectories of length Δt, all starting from the same configuration [16]. Particles colored red in Fig. 1a are those for which the iso-configuration averaged $\bar{\mathbf{r}}_i(\Delta t)$ is more than $0.6\,\sigma$ from $\bar{\mathbf{r}}_i(0)$, where σ is a particle diameter. Smaller enduring displacements are colored by interpolating between red and blue, as noted in the color scale. The figure thus shows that enduring displacements occurring over a short period of time, Δt, take place in sparse localized regions of space. These regions are the excitations [10] in an otherwise rigid material.

Similar pictures illustrating arrangements of enduring displacements are found without iso-configuration averaging. See Fig. 1 of Ref. [10] and also Video 1 and its accompanying figure of Ref. [10]. Iso-configurational averaging serves to burnish those pictures [17]. Without that averaging, localized excitations are already evident but more irregular. Importantly, the excitations, often referred to as soft spots [18], change little in size as the liquid is cooled, and further, provided the system remains liquid, there are no inter-excitation correlations at equal times [10].

Correlations develop over time through dynamics, ultimately leading to static correlations in the non-equilibrium glass. But before considering glass, we focus first on the equilibrium dynamics with Fig. 1b. That picture shows constant-value surfaces of $[a(\mathbf{r}, t)]_{\rm iso}$. The surfaces form connected tubes or lines in space time – excitation lines [19] – indicating that excitations facilitate birth (and death) of adjacent excitations. Larger amplitude fluctuations of the surface occur less frequently than smaller amplitude fluctuations, indicating that the facilitated dynamics is hierarchical [20]. Lowering temperature reduces the number of excitations or soft spots, which reduces the probability that soft spots can connect, which reduces the rate at which the system can relax.

This behavior is found consistently in glass-forming liquids for all temperatures below the onset, i.e., $T < T_{\rm o}$ [10]. Throughout this regime, it is characterized by simple equations for space-time scaling and for the equilibrium distribution of distances between neighboring soft spots, $P_{\rm eq}(\ell)$:

$$\ell/\sigma = (\tau_\ell/\tau_{\rm o})^{1/\tilde{\beta}\gamma}\,. \qquad (2)$$

and

$$P_{\rm eq}(\ell) = \ell_{\rm eq}^{-1} \exp(-\ell/\ell_{\rm eq})\,, \quad \ell_{\rm eq} = \sigma \exp(\tilde{\beta}/d_{\rm f})\,, \qquad (3)$$

Here, $\tilde{\beta} = J_\sigma/T - J_\sigma/T_{\rm o}$, where J_σ is the energy of an excitation with enduring displacements of the characteristic structural length, σ, $1/\tau_\ell$ is the relaxation rate on length scale ℓ, $d_{\rm f}$ is the fractal dimensionality of dynamic heterogeneity, and γ is the proportionality constant for logarithmic growth of excitation energy with respect to length scale [21]. The parabolic law [10–12], $\tau = \tau_{\rm o} \exp(\tilde{\beta}^2\gamma/d_{\rm f})$, follows from space-time scaling, Eq. (2), evaluated at $\ell = \ell_{\rm eq}$.

Contributions to $P_{\rm eq}(\ell)$ with short inter-excitation lengths, $\ell < \ell_{\rm eq}$, come from regions with excitation lines that connect and reorganize. Contributions with $\ell \gg \ell_{\rm eq}$ come from regions of rigidity – the empty regions of Fig. 1b, so-called "bubbles" in space-time [19]. When the liquid transforms into glass, the temporal extents of those bubbles grow to very long times, and excitation lines rarely or never touch, yielding a striped structure of trajectory space [22]. In that case, excitations are no

longer uncorrelated, and a non-equilibrium correlation length, $\ell_{\rm ne}$, gives the average or most probable separation of excitation lines.

Figure 1c shows that the equilibrium glass-forming liquid already contains the seeds of this non-equilibrium correlation length. Specifically, for a 10^6-particle WCA liquid mixture [23] in $d = 3$ at $T = 0.7\,T_{\rm o}$, Fig. 1c contrasts the equilibrium concentration of excitations with that surrounding a dynamically inactive sub-volume. The trajectory length is $t_{\rm obs} = 50\tau \approx 10^3\Delta t$. The net dynamical activity in a sub-volume Δv is $\int_0^{t_{\rm obs}} dt \int_{\Delta v} d\mathbf{r}\, a(\mathbf{r},t)$. For Fig. 1c, we have partitioned the total volume V into cubes, each of size $\Delta v = 125\,V/N$, and computed $Z(r) = \langle a(\mathbf{r})\rangle_{\Delta v}/a$. Here, a is the equilibrium average of $a(\mathbf{r},t)$, and $\langle\cdots\rangle_{\Delta v}$ is that average conditioned on a low activity in the sub-volume at the origin. Similarly, we have computed the radial distribution of mobility, $F(r) = \langle a(\mathbf{r})\rangle_0/ag(r)$, where $g(r)N/V$ is the mean particle density at $\mathbf{r}$ given a particle is at the origin and $\langle\cdots\rangle_0$ is the equilibrium average given a particle at the origin has just then completed an enduring displacement of at least $0.3\,\sigma$. The red lines of Fig. 1c refer to the 0.1% least active sub-volumes. For $F(r)$, that means the central displacing particle is within such a low-activity sub-volume. The equilibrium $Z(r)$ exhibits no structure, and the equilibrium $F(r)$ decays over the length scale of a single excitation. In contrast, the atypical low-activity functions show significant anti-correlation between neighboring excitations.

III. PREPARING GLASSY STATES

The statistical weight for these low-activity regions are enhanced by shifting to a non-equilibrium s ensemble distribution, $P_s[x(t)] \propto P_0[x(t)]\exp(-s\mathcal{A}[x(t)])$ [2–4, 24]. Here, $P_0[x(t)]$ is the equilibrium distribution functional for trajectories $x(t)$ of length $t_{\rm obs}$, and $\mathcal{A}[x(t)]$ is the net dynamical activity [25],

$$\mathcal{A}[x(t)] = \int_V d\mathrm{r} \int_0^{t_{\rm obs}} dt\; a(\mathrm{r},t)\,. \tag{4}$$

For an ergodic equilibrium system, $\mathcal{A} = t_{\rm obs}Va$. Deviations from this equilibrium value are measures of non-ergodic non-equilibrium behavior. Time integrals of other quantities, not just the activity as in Eq. (4), can also serve as suitable order parameters to distinguish ergodic and non-ergodic behavior. Time integration is the crucial feature. Fluctuations are then intimately related to the behavior of time correlators.

Remarkably, for systems at $T < T_{\rm o}$, the marginal equilibrium distribution for $\mathcal{A}$ exhibits fat tails at low activity [1], so that the non-equilibrium mean, $\langle\mathcal{A}\rangle_s$, changes abruptly around a transition value of s. For $s < s^*$, the material is a normal melt, and for $s > s^*$, the material is an inactive amorphous phase – a glass. The abrupt change tends to a discontinuity as $Nt_{\rm obs} \to \infty$. The "glass transition" in the s ensemble (that is, the transition to a non-ergodic state of minimal activity) is thus a first-order transition in the ensemble of trajectories [2–4].

Consider now the "glass transition" defined in the usual experimental way [7] as the point at which the system falls out of equilibrium because relaxation times become longer than practical observation times. (The glass transition defined in this manner is thus not a singularity but a pronounced crossover.) Even more remarkably then, this transition can be obtained via the s ensemble with $t_{\rm obs}$ much shorter than time scales required to produce glass from standard cooling protocols. By cooling at a rate ν, a glass transition occurs at the temperature $T_{\rm g}$, where $\nu^{-1} \approx |d\tau/dT|_{T=T_{\rm g}}$. The time scale for that process is $\tau_{\rm g} = \tau(T_{\rm g})$. The transition freezes excitations separated by the non-equilibrium length, $\ell_{\rm ne} = \ell_{\rm eq}(T_{\rm g})$. From Eq. (2), $\ell_{\rm ne}/\sigma = (\tau_{\rm g}/\tau_{\rm o})^{1/\tilde\beta_{\rm g}\gamma}$. This length must be large if the glass persists for long times. Thus, in view of Eq. (3), $\tilde\beta_{\rm g} > 1$. Typically, $\tau_{\rm g} > 10^{10}\tau_{\rm o}$ and $\ell_{\rm ne} \gtrsim 10\,\sigma$.

On the other hand, with the s ensemble, the same large non-equilibrium length can be obtained with any value of $\tilde\beta$. In that case, from Eq. (2), $\ell_{\rm ne}/\sigma = (t_{\rm obs}/\tau_{\rm o})^{1/\tilde\beta\gamma}$. As such,

$$t_{\rm obs}/\tau_{\rm o} = (\tau_{\rm g}/\tau_{\rm o})^{\tilde\beta/\tilde\beta_{\rm g}}\,. \tag{5}$$

The ratio $\tilde\beta/\tilde\beta_{\rm g}$ can be much smaller than 1. In practice, $\tilde\beta/\tilde\beta_{\rm g} \approx 1/10$. Thus, the simulation time required to prepare a glassy state in the s ensemble, $t_{\rm obs}$, is many orders of magnitude shorter than the time to prepare glass by straightforward cooling, $\tau_{\rm g}$.

IV. ILLUSTRATION WITH THE EAST MODEL

Equation 5 follows from well-tested scaling relationships, and there is some empirical evidence that glasses produced with the s ensemble do indeed coincide with natural structural glass [6, 26]. Nevertheless, this relationship is not yet tested explicitly. Here, we do so for the East model [8], the simplest of models consistent with phenomenology of structural glasses and glass formers [12, 22, 27].

In brief, the East model consists of a $d = 1$ lattice with N sites, each with variables $n_i = 0, 1$. The equilibrium concentration of excitations is $\langle n_i\rangle = c$. At low temperatures, $c \sim \exp(-1/T)$. (We take 1 as the energy scale and length scale for the model.) Sites with $n_i = 1$ can facilitate a spin flip at the adjacent site n_{i+1}. The corresponding transition rates are given for a site i by $k_{i,0\to1} = n_{i-1}c/(1-c)$ and $k_{i,1\to0} = n_{i-1}$. The dynamics of this model is hierarchical [8, 9]. Its structural relaxation slows by twelve orders of magnitude as T decreases from 1 to 0.2 [28], it obeys space-time scaling of Eq. (2) and the parabolic law with $\gamma \approx 1/2\ln 2$ [28–30]. (A different value of γ applies for aging regimes [31].) An equilibrium trajectory of the model is shown in Fig. 2a. Three

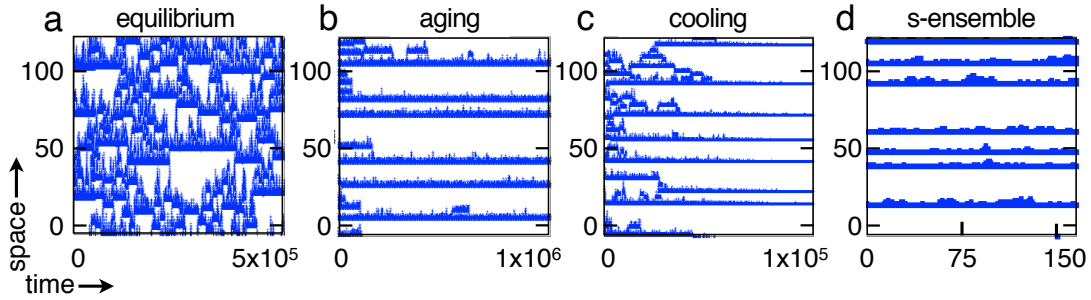

FIG. 2. (Color online) Trajectories of excitations in the East model. (a) Equilibrium dynamics for $T = 0.45$ over a time scale spanning about 50 structural relaxation times at that temperature. (b) Aging dynamics after a quench from $T = 1$ to $T = 0.25$. (c) Cooling at a rate $\nu = 10^{-5}$. (d) Trajectory from the s ensemble at $T = 0.72$ and $s > s^* \approx 10^{-2}$, trajectories running for about 1/2 a structural relaxation time at that temperature.

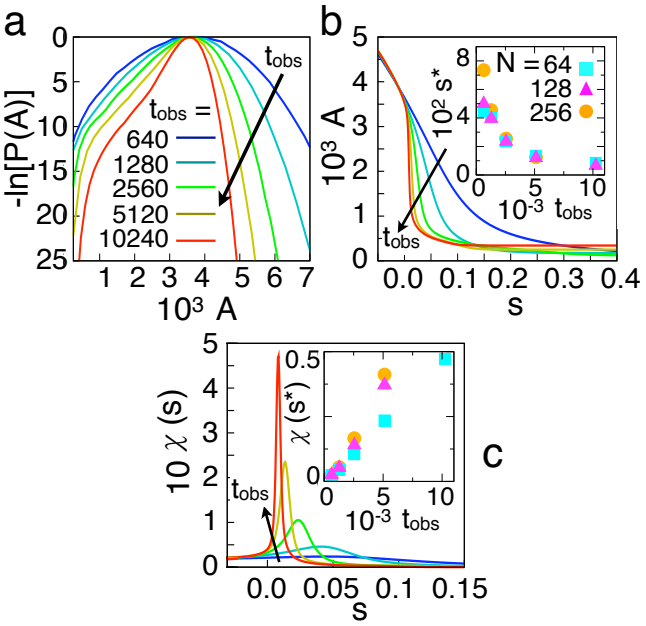

FIG. 3. (Color online) First-order dynamical phase transition in the s ensemble with activity measured in terms of enduring kinks. (a) Probability of observing a trajectory with intensive activity A, for several $t_{\rm obs}$ (arrow indicates the direction of increasing $t_{\rm obs}$) for the $d = 1$ East model at $T = 0.72$ and $N = 64$. (b) A as a function of s for the same systems sampled in (a). The value of s^* is plotted as a function of $t_{\rm obs}$ in the inset for different system sizes N. (c) Susceptibility $\chi(s)$ as a function of s. The inset shows the peak of the susceptibility, $\chi(s^*)$ as a function of $t_{\rm obs}$ for different N.

protocols for preparing non-equilibrium glass states are illustrated in Figs. 2b, 2c and 2d.

In the first, aging, the model is initially equilibrated at $T = 1$ and then instantly quenched to $T = 0.25$, after which it runs at that the low temperature for times $t_{\rm age}$, where $\tau(1) \ll t_{\rm age} \ll \tau(0.25) \approx 3 \times 10^9$. During the time $t_{\rm age}$, the system can relax domains that are smaller than a characteristic length [9, 22] $\ell_{\rm ne} = (t_{\rm age}/\tau_{\rm o})^{1/\tilde{\beta}\gamma}$, with $\tilde{\beta} \approx 3$. We use $t_{\rm age} \approx 10^6$ so as to produce an average non-equilibrium spacing between excitations of about 10.

In the second, cooling, the model is equilibrated at a temperature $T = 1$ and then cooled to zero temperature at a rate of $\nu = 10^{-5}$. A glass transition occurs at the

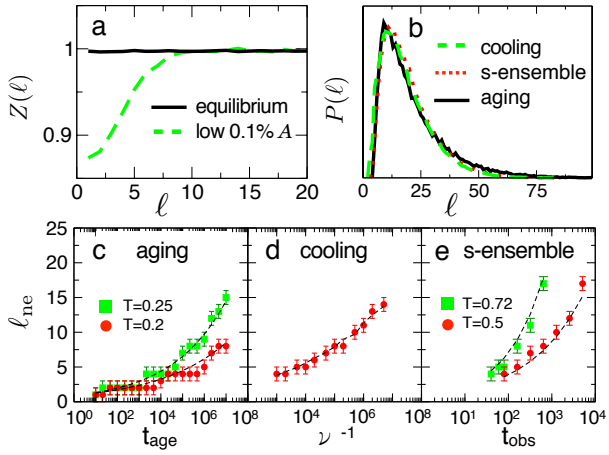

FIG. 4. (Color online) Distributions of East-model glasses. (a) The relative concentration of excitations a distance ℓ from one of the least active sub-regions in the equilibrium model at temperature $T = 0.5$ (b) Distributions of domain lengths $P(\ell)$ for systems aged, cooled and driven with s, all designed to yield $\ell_{\rm ne} \approx 10$. Here, ℓ represents the distance between frozen excitations (called "super-spins"[9]). Superspins were identified by rapidly quenching final configurations, thus removing fleeting short-lengthscale fluctuations and revealing the underlying domain structure. Aging was done at $T = 0.25$ for $t_{\rm age} = 2.5 \times 10^5$ after quenching from $T = 0.4$. Cooling to $T = 0$ was done with a cooling rate of $\nu = 10^{-6}$. s-enemble trajectories were carried out at $T = 0.72$ for a time duration of $t_{\rm obs} = 320$. (c-e) Growth of $\ell_{\rm ne}$ as a function of relevant time variables. Dashed lines in (c) refer to $\ell_{\rm ne} = (t_{\rm age}/\tau_{\rm o})^{1/\tilde{\beta}\gamma}$; dashed line in (d) refers to $\ell_{\rm eq}(T_{\rm g})$; dashed lines in (e) refer to $\ell_{\rm ne} = (t_{\rm obs}/\tau_{\rm o})^{1/\tilde{\beta}\gamma}$.

stage where $1/\nu \approx |d\tau/dT|$, which gives $T_g \approx 0.48$ and thus $\ell_{\rm ne} \approx 10$ and $\tau_{\rm g} \approx 10^6$. In other words, excitations in the glass are frozen in with a typical spacing of about 10, and the time scale to create the material is about 10^6.

The third protocol for preparing a glass state corresponds to using the s ensemble method [1–5]. Aspects of the s ensemble results are detailed in Fig. 3. The s ensemble is sampled according to the methods outlined in Refs. [4, 34]. We use standard transition path sampling with both shooting and shifting moves to sample trajectory space. The s ensemble at each state point is sampled within 20 simulation windows, w, each with a different target value of activity, $\mathcal{A}_w$. Trajectories are accepted or rejected according to a standard umbrella sampling criterion [35], with a harmonic biasing potential acting on the activity for each window, $W = k\left(\mathcal{A}[X] - \mathcal{A}_w\right)^2$, where $\mathcal{A}[X]$ is the total number of enduring kinks for the trajectory X. At the state points considered, optimal sampling is obtained for $k \approx 10^5$. Replica exchange between windows is implemented to facilitate the sampling of glassy states with low activity, which are inherently slowly-evolving. Un-biased statistical averages are obtained using the multi-state Bennet acceptance ratio method [36].

Whereas aging tends to eliminate short domains because larger domains are kinetically frozen, the s ensemble eliminates short domains because of the statistical penalty imposed by the field s. In both cases, domains that are shorter than $\ell_{\rm ne}$ relax on average while larger domains remain intact. For aging, $\ell_{\rm ne} \sim t_{\rm age}^{1/\tilde{\beta}\gamma}$, where $\tilde{\beta}$ coincides with the temperature of the quench. For the s ensemble, $\ell_{\rm ne} \sim t_{\rm obs}^{1/\tilde{\beta}\gamma}$, where $\tilde{\beta}$ coincides with the temperature of the s ensemble trajectories.

The probability density of intensive activity, $A \equiv \mathcal{A}[X]/Nt_{\rm obs}$, is plotted in Fig. 4(a) as a function of $t_{\rm obs}$ for $s = 0$. For all $t_{\rm obs}$, the activity distribution is non-Gaussian and exhibits a fat tail for low values. This is the signature of a low-activity phase that can be accessed by driving the system with s. Fig. 4(b) shows that, for s exceeding a critical value s^* (i.e., the value of s that maximizes $\mathrm{d}A/\mathrm{d}s$), the system undergoes a phase transition into this inactive state. The value of s^* tends to zero as $t_{\rm obs} \to \infty$, as $\mathcal{A}[X]$ grows extensively with time. The sharpness of the transition is quantified by a susceptibility $\chi(s) \equiv \mathrm{d}A/\mathrm{d}s = \langle A^2 \rangle - \langle A \rangle^2$, plotted in Fig. 4(c). The length $\ell_{\rm ne}$ exceeds the system size N in the limit $t_{\rm obs} \to \infty$, and the system forms a single domain of length N. (The final spin cannot be eliminated due to the boundary conditions and facilitation rules.) Activity fluctuations at $s = s^*$ therefore scale proportionally with $Nt_{\rm obs}$, as illustrated in the inset of Fig. 4(c). This scaling is the hallmark of a first-order dynamical phase transition at $s = s^*$. If $\ell_{\rm ne}$ exceeds N, the system undergoes a first order transition to an ideal inactive phase; otherwise, the transition is smooth and the system falls into a striped phase.

The s ensemble protocol produces a similar glass to aging or cooling in a much shorter time. A similar inter-excitation distance is targeted with trajectories run at $T = 0.72$ for which $\tau \approx 300$ and $\tilde{\beta} \approx 0.3$. The glass transition from the cooling protocol occurs at $\tilde{\beta}_{\rm g} \approx 1/(1/2) - 1 = 1$. Accordingly, from Eq. (5), the s ensemble transition for trajectories at $T = 0.72$ produces the glass with $\ell_{\rm ne}$ when $t_{\rm obs} \approx 100$. To apply the s ensemble, we use the total number of enduring kinks as a measure of dynamical activity. An enduring kink at site i is a change in n_i that persists for at least a mean exchange time [27]. At $T = 0.72$ and $t_{\rm obs} \approx 100$, for system size N chosen, the s ensemble glass transition occurs at $s^* \approx 10^{-2} = O(1/N)$ [33].

Figure 4 compares the non-equilibrium correlation lengths and distribution functions for the three different preparation protocols. It also shows $Z(\ell)$, which is the relative concentration of enduring kinks a distance ℓ from the 0.1% least-active domains of the equilibrium East model. It exhibits a correlation hole in a fashion similar to the analogous $Z(r)$ in the WCA mixture, Fig. 1. The East model thus illustrates how preparation of glass, which necessarily requires long physical times, can be accomplished in simulation in much shorter times through application of the s ensemble. Equation (5) provides the key for understanding prior successes in preparing glassy states through applications of the s ensemble in atomistic models. However, if the simulation box size, L, is smaller than target non-equilibrium length, the s ensemble method prepares a distribution of glassy states, all of which correspond to inactive domains in glasses with $\ell_{\rm ne} > L$.

Natural dynamics changes ℓ continuously, and at the point where the system falls out of equilibrium $\ell_{\rm ne} = \ell_{\rm eq}$. The equilibrium length, $\ell_{\rm eq} = \langle \ell \rangle$, is equivalent to a or c. Because the length scale changes continuously as a glass former falls out of equilibrium, the glass transition has the appearance of a second-order transition. However, the time-integrated order parameters, the distribution of ℓ, and the connection between ℓ and c, all change abruptly. The change becomes singular in the limit of infinite time, manifesting the first-order non-equilibrium transition that underlies the glass transition.

V. CONCLUSION

This paper provides two new results that seem central for understanding the nature of glass and the computational methods available for modelling it. The first result is that the spatial distribution of excitations in a glass prepared either by finite-rate cooling or by quenching and long-time aging is the same as that for rare glassy configurations of an equilibrium system, the latter captured efficiently with s ensemble re-weighting. This result we demonstrated explicitly with the East model, see Fig. 4, but we expect it to be valid more broadly for glass formers given the scaling relationships we have discussed. Furthermore, the second result of this paper supports this

expectation. Fig. 1 demonstrates that rare mesoscopic domains of low activity that occur in the supercooled regime of atomistic glass formers exhibit non-trivial inter-excitation correlations: each excitations is surrounded by a correlation hole, within which another excitation is improbable. This is a signature at the mesoscopic level of the anti-correlation between excitations that we expect to see as typical in the non-equilibrium glass (in contrast to excitations in liquid configurations which are distributed randomly, cf. Ref. [10]).

Further demonstration of our prediction of a non-equilibrium length, and the equivalence of standard and s ensemble prepared glasses, with atomistic molecular simulations might press the limits of current technology. For example, for a $d = 3$ mixture like that considered in Fig. 1c, we estimate from Eqs. (2) and (5) and data provided in Ref. [10] that clear emergence of the large correlation length characteristic of a glass will require cooling a trajectory of 10^7 particles over 10^{10} integrations steps. Corroboration with experiment might be less formidable, either through imaging sub volumes of colloidal glass formers driven to a glassy state with finite rate compression, or through scattering from molecular glass formers driven to a glassy state by finite-rate cooling, comparing the glass with the melt over large length scales.

ACKNOWLEDGMENTS

We thank D.T. Limmer, R.L. Jack, P. Sollich, T. Speck and Y.S. Elmatad for helpful discussions. Salaries were supported by the Director, Office of Science, Office of Basic Energy Sciences, and by the Division of Chemical Sciences, Geosciences, and Biosciences of the U.S. Department of Energy at LBNL, by the Laboratory Directed Research and Development Program at Lawrence Berkeley National Laboratory under Contract No. DE-AC02-05CH11231, and by Leverhulme Trust grant no. F/00114/BG. NSF award CHE-1048789 provided computational resources.

APPENDIX A: DEMONSTRATION OF NO CRYSTALLIZATION AT SUPERCOOLED CONDITIONS STUDIED

When considering dynamical phase transitions it is important to rule out crystallization [3]. The systems we consider have never been known to crystallize during a brute force simulation at the state points under consideration, but as described below we have taken all precautions to rule out this possibility. (When perturbed by umbrella sampling, much smaller systems – like those studied with s ensemble calculations – can crystallize if not biased against. But those occurrences are rare events in a small system, not the behaviour found in straightforward simulation of a large system.)

Binary mixtures tend to phase-separate when they crystallize. At high densities like those we consider, packing constraints dictate that such crystals would likely be close-packed—hexagonal in two dimensions (2D) and hcp and/or fcc in three dimensions (3D). Snapshots of the 2D liquid, such as the one of Fig. 1(a) above, do show some hexagonal clusters of particles. These however are not an indication of incipient crystallization, as they do not grow with time, but rather obey a typical size distribution. The same occurs for the 3D system: there are some local clusters, but they fluctuate in and out and do not grow.

The methods we used to establish these observations were the following. Crystal-like clusters of size N are measured using the methods developed for observing crystal nucleation in simulations [37, 38]. These methods measure the degree of alignment between the first neighbor shell of neighboring particles, where strong alignment indicates a local crystal-like environment. The spatial density of neighbors is expanded in spherical harmonics, chosen to match the rotational symmetry of the neighbor shell clusters. (In 2D, we substitute the Fourier decomposition for the original spherical harmonics decomposition.) We consider 4-fold and 6-fold symmetry independently, which are sensitive to close-packed crystals in 3D [39], as well as linear combinations of n-fold symmetries with $4 \leq n \leq 12$ to account for any other unexpected crystal structures. Fig. 5(a) shows 6-fold hexagonal clusters detected in this way in the 2D system. We check for the possibility of slow coarsening of the crystalline phase by comparing the both the size of the largest cluster in the system and the cluster size distribution at the beginning and end of the runs, that is, with a time separation of several 10^2 alpha-relaxation times. Over this length of time, we found that neither the largest cluster nor the clusters size distribution $P(N)$ change. The cluster size distributions for 6-fold clusters are shown in Figs. 5(b,c) for the 2D and 3D systems. We observe similar trends for other symmetries as well. In summary, all standard measures indicate that neither the 2D nor the 3D systems we consider in this paper are crystallizing at the conditions for which we study supercooled liquid behavior.

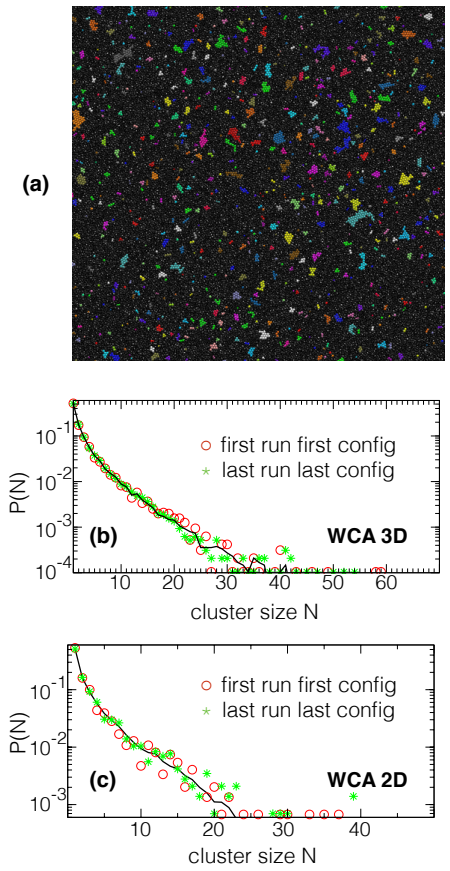

FIG. 5. (Color online) (a): A typical configuration of the 2D system contains many hexagonal clusters (colored). The clusters are locally stable. (b,c): Probability of 6-fold clusters (3D WCA) and hexagonal clusters (2D WCA) at different times. The cluster distributions do not exhibit net growth with time at the state points considered in the main text. The last configuration is separated in time from the first configuration by more than 10^2 structural relaxation times.

[1] M. Merolle, J. Garrahan, and D. Chandler, Proc. Natl. Acad. Sci. USA **102**, 10837 (2005).

[2] J. P. Garrahan, R. L. Jack, V. Lecomte, E. Pitard, K. van Duijvendijk, and F. van Wijland, Phys. Rev. Lett. **98**, 195702 (2007).

[3] L. O. Hedges, R. L. Jack, J. P. Garrahan, and D. Chandler, Science **323**, 1309 (2009).

[4] T. Speck and D. Chandler, J. Chem. Phys. **136**, 184509 (2012).

[5] T. Speck, A. Malins, and C. P. Royall, Phys. Rev. Lett. **109**, 195703 (2012).

[6] R. L. Jack, L. O. Hedges, J. P. Garrahan, and D. Chandler, Phys. Rev. Lett. **107**, 275702 (2011).

[7] For general reviews on the glass transition problem and on different theoretical approaches see, e.g., M. Ediger, C. Angell, and S. Nagel, J. Phys. Chem. **100**, 13200 (1996); V. Lubchenko and P. G. Wolynes, Annu. Rev. Phys. Chem. 58, 235 (2007); A. Cavagna, Phys. Rep. **476**, 51 (2009); D. Chandler and J. P. Garrahan, Annu. Rev. Phys. Chem. **61**, 191 (2010); K. Binder and W. Kob, *Glassy materials and disordered solids* (World Scientific, 2011); L. Berthier and G. Biroli, Rev. Mod. Phys. **83**, 587 (2011); G. Biroli and J.P. Garrahan, J. Chem. Phys. **138**, 12A301 (2013).

[8] J. Jäckle and S. Eisinger, Z. Phys. B **84**, 115 (1991).

[9] P. Sollich and M. R. Evans, Phys. Rev. E **68**, 031504 (2003).

[10] A. S. Keys, L. O. Hedges, J. P. Garrahan, S. C. Glotzer, and D. Chandler, Phys. Rev. X **1** (2011).

[11] J. P. Garrahan and D. Chandler, Proc. Natl. Acad. Sci. **100**, 9710 (2003).

[12] Y. S. Elmatad, D. Chandler, and J. P. Garrahan, J. Phys. Chem. B **113**, 5563 (2009).

[13] Y. S. Elmatad, D. Chandler, and J. P. Garrahan, J. Phys. Chem. B **114**, 17113 (2010).

[14] $T_{\rm o}$ is the crossover temperature below which dynamics is spatially heterogeneous. Below that temperature, the structural relaxation time is super-Arrhenius, obeying the parabolic law [11, 12], and above that temperature, the structural relaxation time is Arrhenius or sub-Arrhenius. Reversible transport properties at very low temperatures can be predicted quantitatively by extrapolation from behavior near but below $T_{\rm o}$ [10, 13]. Thus, we see is no evidence for another dynamical crossover in reversible supercooled glass forming liquids.

[15] F. H. Stillinger and T. A. Weber, Phys. Rev. A **25**, 978 (1982).

[16] A. Widmer-Cooper, P. Harrowell, and H. Fynewever, Phys. Rev. Lett. **93**, 135701 (2004).

[17] Ref. [16] considered iso-configurational averaging with $\mathbf{r}_i(t)$ rather than with $\bar{\mathbf{r}}_i(\Delta t)$. In that case, vibrations obscure structure, especially for short trajectories. Burnishing with $\bar{\mathbf{r}}_i(\Delta t)$, not $\mathbf{r}_i(\Delta t)$, produces a vivid picture.

[18] M. L. Manning and A. J. Liu, Phys. Rev. Lett. **107**, 108302 (2011).

[19] J. P. Garrahan and D. Chandler, Phys. Rev. Lett. **89**, 35704 (2002).

[20] R. G. Palmer, D. L. Stein, E. Abrahams, and P. W. Anderson, Phys. Rev. Lett. **53**, 958 (1984).

[21] For $d = 1$, $d_{\rm f} = 1$. For dimensions $d = 2$ and 3, numerics [10] finds $d_{\rm f} \approx 1.8$ and 2.4, respectively, and γ is of order one, with a specific value that is system dependent.

[22] A. S. Keys, J. P. Garrahan, and D. Chandler, Proc. Natl. Acad. Sci. USA **110**, 4482 (2013).

[23] L. O. Hedges, L. Maibaum, D. Chandler, and J. P. Garrahan, J. Chem. Phys. **127**, 211101 (2007).

[24] V. Lecomte, C. Appert-Rolland, and F. van Wijland, J. Stat. Phys. **127**, 51 (2007).

[25] There is significant freedom in the specific choice of dynamical activity. For example, a suitable alternative [4] is $\mathcal{A}[x(t)] = \sum_i \sum_t \theta(|\bar{\mathbf{r}}_i(t+\Delta t) - \bar{\mathbf{r}}_i(t)| - \sigma)$, where σ is a particle diameter or a fraction of a particle diameter, $\theta(\cdots)$ is the unit Heaviside function, the sum on i is over all particles, and the sum on t is over time intervals of width Δt extending from 0 to $t_{\rm obs}$.

[26] D. T. Limmer and D. Chandler, Proc. Natl. Acad. Sci. USA. **111**, 9413 (2014).

[27] Y. S. Elmatad and A. S. Keys, Phys. Rev. E **85**, 061502 (2012).

[28] D. J. Ashton, L. O. Hedges, and J. P. Garrahan, J. Stat. Mech. Theor. Exp. **2005**, P12010 (2005).

[29] D. Aldous and P. Diaconis, J. Stat. Phys. **107**, 945 (2002).

[30] P. Chleboun, A. Faggionato, and F. Martinelli, J. of Stat. Mech. Theor. Exp. **2013**, L04001 (2013).

[31] When ℓ is short compared to $\ell_{\rm eq}$ (i.e., the regime most relevant for aging protocols) $\gamma = 1/\ln 2$ [32]. For longer ℓ, γ is reduced by entropic effects to a limiting value $1/2\ln 2$ [30].

[32] P. Sollich and M. R. Evans, Phys. Rev. Lett. **83**, 3238 (1999).

[33] T. Bodineau, V. Lecomte, and C. Toninelli, J. Stat. Phys. **147**, 1 (2012).

[34] R. L. Jack, J. P. Garrahan, and D. Chandler, J. Chem. Phys. **125**, 184509 (2006).

[35] G. M. Torrie and J. P. Valleau, J. Comp. Phys. **23**, 187 (1977).

[36] M. R. Shirts and J. D. Chodera, J. Chem. Phys. **129** (2008).

[37] P.R. ten Wolde1, M.J. Ruiz?Montero and D. Frenke, J. Chem. Phys. **104**, 9932 (1996).

[38] S. Auer and D. Frenkel, Nature **409**, 1020 (2001).

[39] P.J. Steinhardt, D.R. Nelson and M. Ronchetti, Phys. Rev. B **28**, 784 (1983).